Research Square

Preprints are preliminary reports that have not undergone peer review.
They should not be considered conclusive, used to inform clinical practice,
or referenced by the media as validated information.

Enhanced Supercapacitive Performance of Fe-Doped CuO Nanostructured Thin Films Synthesized via Ultrasonic Spray Pyrolysis

Demet İSKENDEROĞLU
Kazım Karabekir Education Faculty, Atatürk University
Kübra ÇINAR DEMİR
Atatürk University
Harun GÜNEY
Atatürk University
Muhammed Emin GÜLDÜREN
megulduren@agri.edu.tr
Ağrı İbrahim Çeçen University
Sibel Morkoç KARADENİZ
Erzincan Binali Yıldırım University
Aykut ASTAM
Erzincan Binali Yıldırım University

Research Article

Keywords: Fe doped CuO, supercapacitor, CV and GCD

Posted Date: April 10th, 2026

DOI: https://doi.org/10.21203/rs.3.rs-8865174/v1

License: This work is licensed under a Creative Commons Attribution 4.0 International License.
Read Full License

Additional Declarations: No competing interests reported.

Enhanced Supercapacitive Performance of Fe-Doped CuO Nanostructured Thin Films Synthesized via Ultrasonic Spray Pyrolysis

Demet İSKENDEROĞLU[1], Kübra ÇINAR DEMİR[2], Harun GÜNEY[3], Muhammed Emin GÜLDÜREN[4*], Sibel Morkoç KARADENİZ[5], Aykut ASTAM[5]

[1]*Kazım Karabekir Education Faculty, Department of Science Education,*
Atatürk University, Erzurum-Turkey

[1]*Department of Science Education,*
Atatürk University, Erzurum-Turkey

[2]*Department of Physics, Science Faculty,*
Atatürk University, Erzurum-Turkey

[3]*Vocational School Technical Sciences, Department of Electric and Energy,*
Atatürk University, Erzurum-Turkey

[4]*Vocational School, Department of Electric and Energy,*
Ağrı İbrahim Çeçen University, Ağrı-Turkey

[5]*Department of Physics, Art & Science Faculty,*
Erzincan Binali Yıldırım University, Erzincan-Turkey

[*]Corresponding author e-mail: megulduren@agri.edu.tr

Abstract

CuO nanostructured thin films, both undoped and Fe-doped, were successfully deposited onto ITO substrates using the ultrasonic spray pyrolysis (USP) technique. The structural, morphological, optical, and electrochemical characteristics of CuO were systematically investigated as a function of Fe incorporation. X-ray diffraction results verified the formation of the monoclinic CuO phase. However, noticeable changes in peak intensity and crystallite size were observed after Fe addition. Moreover, SEM images revealed that Fe doping modified the surface morphology and promoted the growth of larger polyhedral grains. Elemental mapping further verified the uniform distribution of Fe within the CuO matrix. Optical measurements showed an increase in absorbance and a slight widening of the band gap with increasing Fe content. In addition, photoluminescence intensity decreased after doping, indicating changes in defect structure and charge recombination behavior. The electrochemical performance was evaluated using cyclic voltammetry, galvanostatic charge–discharge, and impedance spectroscopy in 1 M KOH electrolyte. The Fe-doped CuO electrodes exhibited significantly enhanced specific capacitance compared to undoped CuO. This improvement was attributed to increased surface activity and improved charge transfer properties. Thus, Fe

incorporation effectively enhanced the electrochemical behavior of CuO thin films, making them promising candidates for supercapacitor applications.

Keywords: Fe doped CuO, supercapacitor, CV and GCD

Introduction

Semiconductor materials based on metal oxides have gained significant interest owing to their distinctive physical and chemical characteristics. Among them, copper oxides stand out because of their low toxicity, good chemical stability, and wide natural availability. Copper oxides commonly exist in two stable phases at room temperature, namely CuO (tenorite) and Cu_2O (cuprite). In addition, CuO exhibits p-type conductivity, which originates from copper vacancies or oxygen-related defects within its structure. Therefore, CuO has been widely studied for applications such as photovoltaic devices [1, 2], gas and humidity sensors [3, 4], high-temperature superconducting devices [5], and supercapacitors [6].

Recently, electrochemical supercapacitors have gained significant interest as advanced energy storage systems. They provide fast charge–discharge capability, long cycle life, high power density, and safe operation. Moreover, they are suitable for applications including hybrid vehicles, portable electronics, and military technologies [1, 2]. Based on their charge storage mechanisms, supercapacitors are commonly classified as electric double-layer capacitors, pseudocapacitors, and hybrid capacitors [3–5]. Electric double-layer capacitors store energy through electrostatic charge accumulation at the electrode–electrolyte interface. In contrast, At or near the electrode surface take place the reversible faradaic redox reactions through which pseudocapacitors operate.

By the properties of the electrode material is largely determined the performance of a supercapacitor [6]. Therefore, developing new electrode materials with improved conductivity and higher surface activity is essential. Transition metal oxides have attracted attention for this purpose because they exhibit multiple oxidation states and reversible redox behavior. Among them, CuO is considered a promising candidate due to its electrochemical activity and low production cost. However, its practical performance is often limited by moderate electrical conductivity and restricted ion diffusion.

To modify the structural and electronic properties of semiconductor oxides is considered doping an effective strategy. The incorporation of foreign ions can influence crystallinity, defect concentration, charge transport, and surface reactivity. In particular, Fe doping has the potential

to enhance redox reactions and improve electrochemical behavior. Fe ions may alter the electronic structure of CuO and increase the number of active sites. Thus, Fe incorporation can contribute to improved charge transfer characteristics and higher specific capacitance.

In this study, CuO nanostructured thin films, both undoped and Fe-doped, were grown on ITO substrates by the ultrasonic spray pyrolysis method. Their morphological, structural, optical, and electrochemical attributes were systematically analyzed. Special attention was given to their supercapacitive behavior in an alkaline electrolyte. Thus, this work aimed to elucidate how Fe doping influenced and improved the electrochemical performance of CuO thin film electrodes.

Experimental

To evaluate the influence of Fe incorporation, structural, morphological, optical, and electrochemical characterizations were carried out. To examine phase formation and crystallinity was performed the X-ray diffraction (XRD) analysis. Using energy dispersive X-ray spectroscopy (EDX) and scanning electron microscopy (SEM) were analyzed the surface morphology and elemental composition. Optical properties were investigated by UV–Vis spectroscopy and photoluminescence (PL) measurements. Using cyclic voltammetry (CV), galvanostatic charge–discharge (GCD), and electrochemical impedance spectroscopy (EIS) techniques was assessed the electrochemical performance.

Using the ultrasonic spray pyrolysis technique were fabricated pure and Fe-doped CuO thin films on soda lime glass substrates. Copper nitrate trihydrate ($Cu(NO_3)_2 \cdot 3H_2O$, Sigma-Aldrich, 99%) and iron nitrate nonahydrate ($Fe(NO_3)_3 \cdot 9H_2O$, Sigma-Aldrich, 99%) were used as precursor materials. A 0.1 M copper nitrate solution was first prepared in distilled water. For doping, iron nitrate was added to the solution at concentrations of 0.5 and 1 wt%. Before deposition, the glass substrates were cleaned sequentially in distilled water, acetone, and diluted HCl solution. On a heated platform maintained at 400 °C were then placed the cleaned substrates. The temperature was monitored using a thermocouple with an accuracy of ±5 °C.

The precursor solution was atomized using an ultrasonic nebulizer operating at a frequency of 100 kHz. The generated aerosol droplets were transported to the heated substrate surface by filtered compressed air. During deposition, the solution flow rate was adjusted to 1.25 mL/min, and the total sprayed volume was 50 mL. The substrate holder was rotated at 20 rpm to ensure uniform film formation. At 35 cm was maintained the distance between the spray nozzle and

the substrate, and to 45° was adjusted the spray angle. Using the gravimetric weight difference method was determined the thickness of the deposited films. All samples exhibited an average thickness of approximately 350 nm. Additional experimental details regarding instrumentation and measurement conditions were consistent with those reported in our previous studies [7–9].

Results and Discussion

The X-ray diffraction measurements were performed to assess the influence of Fe incorporation on the crystal structure of the CuO thin films. The diffraction patterns of the undoped and Fe-doped samples were shown in figure 1. The undoped CuO film exhibited characteristic diffraction peaks at approximately 32.99° (110), 35.99° (002), 39.19° (111), 53.96° (020), and 68.43° (220). These reflections were consistent with the monoclinic CuO phase (JCPDS No. 02-1225). Therefore, the formation of phase-pure CuO in the undoped sample was confirmed. With the introduction of Fe, noticeable variations in peak intensities were observed. The diffraction peaks became more pronounced as the Fe concentration increased, which suggested modifications in crystallinity. However, additional reflections appeared at around 49.32° and 66.68° in the Fe-doped samples. These peaks corresponded to Fe-related oxide phases (γ-Fe_2O_3) according to JCPDS No. 79-0007. A similar observation was previously reported by Youxia Li et al. [10]. Thus, the presence of Fe influenced both phase composition and structural characteristics.

In order to examine the structural modifications in greater detail, several crystallographic parameters were calculated from the XRD data. The interplanar spacing (d), average crystallite size (D), microstrain (ε) and dislocation density (δ) were determined using the following equations:

$$n\lambda = 2dsin\theta \quad (1)$$

$$D = \frac{k\lambda}{\beta \cos\,\theta} \quad (2)$$

$$\delta = \frac{1}{D^2} \quad (3)$$

$$\varepsilon = \frac{\beta}{4tan\theta} \quad (4)$$

where, θ is the Bragg diffraction angle, k is the Scherrer constant (0.9), λ is the wavelength of the X-ray (=1.54 Å), β is the FWHW, n is the order of the diffracted beam,.

In Table 1 were summarized the calculated structural parameters The crystallite size (D) was found to decrease progressively with increasing Fe content. This reduction indicated that Fe incorporation induced slight lattice distortion and hindered grain growth. Similar behavior has been reported in the literature [11]. In addition, microstrain (ε) and the dislocation density (δ) values increased as the dopant concentration rose. Since these parameters are directly related to structural imperfections, their increase suggested a gradual deterioration in crystallinity with Fe addition [12]. Therefore, although Fe doping enhanced certain diffraction peak intensities, it also introduced structural strain and defect formation within the CuO lattice. Overall, the XRD analysis demonstrated that Fe incorporation significantly modified the microstructural properties of CuO thin films.

The undoped and Fe-doped CuO thin films were characterized by SEM coupled with EDX to evaluate their surface morphology and elemental composition. The corresponding micrographs and spectra are presented in figure 2(a–c). The undoped CuO film exhibited a polyhedron-like morphology with grains distributed in multiple orientations. In addition, relatively smaller and round-shaped particles were observed between larger grains. These morphological observations were consistent with the structural tendencies identified from the XRD analysis. The coexistence of larger faceted grains and smaller rounded particles suggested the contribution of different crystallographic orientations. Specifically, the dominant (002) and (111) planes were associated with larger faceted grains, whereas the (110), (020), and (220) orientations were likely related to the smaller structures. Upon Fe incorporation, noticeable morphological changes were recorded. For the 0.5 wt% Fe-doped sample (figure 2b), the grains appeared more defined and exhibited an increase in average size compared to the undoped film. Furthermore, when the Fe concentration was increased to 1 wt% (figure 2c), the polyhedral grains became more prominent and further enlarged. Therefore, Fe doping clearly influenced grain growth behavior and surface texture. Similar grain morphologies have been reported by Singh et al. [13] and Thi et al. [14], which supported the reliability of the present observations. To the observed grain enlargement and morphological modifications was attributed the incorporation of Fe ions into the CuO lattice. The substitutional or interstitial occupation of Fe at Cu sites likely modified the nucleation and growth kinetics during film formation. Moreover, the presence of smaller nanoparticles within the structure was beneficial for charge transport. Reduced particle size shortened the diffusion path length for electrons (e^-), which could enhance electrochemical activity. Thus, Fe-doped CuO thin films were considered favorable for both gas sensing and supercapacitor applications [15,16].

In figure 2, Elemental mapping and the EDX spectra further confirmed the successful incorporation of Fe into the CuO matrix. The undoped sample exhibited only Cu and O signals, indicating proper stoichiometric formation. In contrast, Fe-doped samples displayed additional Fe peaks while maintaining appropriate O/Fe/Cu ratios. The uniform spatial distribution of Fe within the films demonstrated homogeneous doping without significant phase segregation. Therefore, the EDX results verified the compositional integrity of the synthesized samples. Overall, SEM and EDX analyses revealed that Fe incorporation modified the surface morphology, increased grain size, and successfully integrated into the CuO structure, which was expected to influence electrochemical behavior.

The room-temperature photoluminescence spectra of the undoped and Fe-doped CuO thin films are presented in figure 3. The PL analysis was performed to evaluate the optical emission behavior and defect-related transitions within the CuO structure. All samples exhibited three main emission features under 325 nm excitation. A strong green emission band was observed around 555 nm. In addition, a violet emission near 390 nm and a red emission around 730 nm were detected. These emission bands were characteristic of CuO-based nanostructures and were consistent with previous reports [17–25]. To near-band-edge recombination was attributed the emission peak located at approximately 390 nm. This transition was associated with the intrinsic band structure of CuO and indicated band-to-band electron–hole recombination processes. The green emission centered at 555 nm was related to defect levels within the CuO lattice. Due to the presence of copper vacancies, CuO intrinsically classified as a p-type semiconductor. Therefore, the 555 nm emission was associated with deep-level defects originating from these intrinsic structural imperfections [26]. Such defect states acted as recombination centers within the band gap. The red emission band observed near 730 nm was attributed to oxygen vacancy-related transitions. These vacancies facilitated recombination processes between trapped electrons and holes, leading to defect-mediated luminescence [24–28]. Thus, the PL spectrum reflected the defect structure of the synthesized films. Upon Fe incorporation, a noticeable reduction in PL intensity was recorded. This decrease suggested changes in defect concentration and recombination dynamics. The reduction in emission intensity was associated with modifications in crystallite size and structural disorder, as also indicated by the XRD results. The presence of Fe ions likely introduced additional non-radiative recombination centers, which suppressed radiative transitions. Therefore, Fe doping altered the defect structure and optical recombination behavior of CuO thin films. The PL analysis clearly demonstrated that impurity

incorporation influenced the electronic transitions and defect-mediated emission characteristics.

Using UV–Vis spectroscopy at room temperature were examined the optical properties of the undoped and Fe-doped CuO thin films. In figure 4. the absorbance spectra recorded within the wavelength range of 600–900 nm. In the visible region was exhibited a characteristic absorption profile by the undoped CuO film. With increasing Fe concentration, a noticeable enhancement in absorbance intensity was observed. Therefore, Fe incorporation influenced the light–matter interaction behavior of the CuO thin films. The increase in optical absorption suggested modifications in electronic structure and defect-related transitions within the material. The Tauc relation for direct allowed transitions was employed to estimate the optical band gap energy (E_g):

$$(\alpha h\nu)^2 = A(h\nu - E_g) \quad (5)$$

where hν denoted the photon energy, α represented the absorption coefficient, E_g corresponded to the bandgap energy and A was constant. The band gap values were determined by extrapolating the linear region of the $(\alpha h\nu)^2$ versus hν plot to the photon energy axis at $(\alpha h\nu)^2 = 0$, as illustrated in figure 5. The undoped CuO film exhibited a band gap energy of 1.72 eV. After Fe incorporation, the band gap slightly increased to 1.74 eV for 0.5 wt% Fe doping and 1.76 eV for 1 wt% Fe doping. With increasing Fe content, a gradual widening of the band gap was detected, indicating that impurity incorporation altered the electronic band structure. This behavior could be attributed to lattice distortion, defect modification, and possible changes in carrier concentration induced by Fe ions. Therefore, Fe doping influenced not only structural and morphological characteristics but also the optical transition behavior of the CuO thin films. Therefore, the UV–Vis analysis demonstrated that Fe incorporation modified absorption behavior and slightly shifted the optical band gap toward higher energy values.

By cyclic voltammetry measurements in 1 M KOH electrolyte using a three-electrode configuration was investigated the electrochemical behavior of the undoped and Fe-doped CuO thin film electrodes. The voltammograms recorded at scan rates of 10, 20, 30, 40, 50, and 100 mV/s are presented in figure 6(a) and 6(b). Into the charge storage mechanism and the redox activity of the electrodes provided insight the CV curve. The current response varied systematically with scan rate, reflecting the kinetics of the electrochemical reactions occurring at the electrode–electrolyte interface. An increase in current density was observed as the scan rate increased, which indicated enhanced polarization behavior. The general shape of the CV

curves suggested pseudocapacitive behavior dominated by reversible faradaic redox reactions. The electrochemical response depended strongly on scan rate, potential window, electrolyte composition, and electrode characteristics. Therefore, the morphology and dopant concentration of the films played a significant role in determining capacitance performance. The specific capacitance values calculated from the CV curves were summarized in Table 2. For the undoped CuO electrode, the capacitance decreased gradually as the scan rate increased. This behavior was attributed to insufficient ion diffusion at higher scan rates. At elevated sweep speeds, the electrolyte ions had limited time to penetrate the inner active regions of the electrode, resulting in reduced effective utilization of the material. In contrast, the Fe-doped CuO electrode exhibited a different trend. The specific capacitance increased up to 20 mV/s and then decreased at higher scan rates. This improvement at lower scan rates suggested that Fe incorporation enhanced charge transfer efficiency and provided additional electrochemically active sites. However, similar to the undoped sample, capacitance decreased at higher scan rates due to diffusion limitations. All in all, a significant enhancement in specific capacitance was observed after Fe doping, as clearly demonstrated in figure 6(c). The improved performance was associated with structural modification, increased surface activity, and improved electrical conductivity induced by Fe incorporation. These findings were consistent with previous electrochemical studies reported in the literature [29–32].

The charge–discharge characteristics of the undoped and 1% Fe-doped CuO electrodes were evaluated using galvanostatic charge–discharge measurements in 1 M KOH electrolyte. The corresponding curves recorded at various current densities are shown in figure 7(a) and 7(b). Both electrodes exhibited charge–discharge profiles resembling quasi-linear and symmetric behavior, indicating reversible electrochemical processes. Efficient ion exchange between the electrolyte and the electrode surface during the redox reactions was indicated by the nearly symmetric shape of the curves. In addition, with the internal resistance present in the electrode system was associated the small IR drop detected at the beginning of the discharge process. To assess cycling stability, repeated charge–discharge measurements were conducted for 250 cycles at a current density of 1 A/g. The stable profile of the curves indicated good electrochemical reversibility and structural integrity of the electrodes.The capacitance value (C_s) with the GCD state was calculated by the following equation:

$$C_s = \frac{I}{m.\frac{dV}{dt}} = \frac{I\Delta t}{m.\Delta V} \qquad (6)$$

The calculated capacitance values are listed in Table 2. For the undoped CuO electrode, the specific capacitance decreased from 77 F/g to 2 F/g as the current density increased. Similarly, the Fe-doped CuO electrode exhibited a decrease from 330 F/g to 107 F/g at higher current densities. This decline at elevated current density was attributed to insufficient time for electrolyte ions to access all electrochemically active regions, particularly within pores and inner surfaces. Therefore, only part of the electrode effectively contributed to charge storage at high current density conditions [29–32]. During the charge–discharge process, K^+ ions in the electrolyte participated in charge transfer reactions with Cu species at the electrode surface. The applied current density strongly affected the extent and rate of these redox reactions. At lower current density (1 A/g), the Fe-doped electrode exhibited longer discharge times, which reflected improved charge storage capability. The improved capacitance behavior of the Fe-doped CuO electrode was attributed to enhanced conductivity and increased electrochemically active surface contributions induced by Fe incorporation. Similar trends were reported for doped CuO-based electrodes in previous studies [33–36]. In addition, the literature reported that Fe-doped CuO electrodes could reach their highest capacity at a scan rate of 5 mV/s and a current density of 0.5 A/g under optimized conditions [37]. Thus, the present results were consistent with earlier findings and further supported the beneficial role of Fe incorporation in CuO electrode systems.

To further evaluate the charge transfer characteristics of the undoped and 1% Fe-doped CuO thin film electrodes, electrochemical impedance spectroscopy measurements were conducted. The impedance spectra were recorded in 0.1 M KOH electrolyte over a frequency range of 0.01 Hz to 100 kHz at room temperature. The corresponding Nyquist plots are presented in Figure 7(c). In the high-frequency region, a semicircular feature was exhibited by the Nyquist plot, followed at lower frequencies by an almost linear portion. With the charge transfer resistance occurring at the electrode–electrolyte interface was associated the semicircle detected in the high-frequency domain. A smaller semicircle diameter indicated lower interfacial resistance and faster electron transfer kinetics. In contrast, an increase in semicircle diameter reflected slower charge transport behavior. For the Fe-doped CuO electrode, the semicircle diameter was comparatively reduced, suggesting improved conductivity and enhanced interfacial charge transfer. This improvement was attributed to structural and electronic modifications induced by Fe incorporation. At lower frequencies, the linear portion of the Nyquist plot represented diffusion-controlled processes within the electrode material. The slope of this region was related to ion diffusion behavior. The impedance response also reflected contributions from

surface roughness, non-uniformity, and possible inhomogeneous current distribution across the electrode surface. Therefore, the capacitive behavior was not ideally homogeneous, which was consistent with the observed constant phase element (CPE) behavior. It should be noted that several resistive components contributed to the overall impedance. These included ion diffusion resistance at the electrode–solution interface, surface film resistance, and possible contributions from intermediate species formed during electrochemical reactions. The difference between the intercepts at high and low frequencies along the real impedance axis corresponded to the overall polarization resistance of the system. To quantitatively analyze the impedance response, the experimental data were fitted using the ZView software with a Randles equivalent circuit model. In this model, Rs represented the solution resistance, Rp denoted the polarization resistance, and CPE described the non-ideal capacitive behavior of the electrode surface. The equivalent series resistance (Rs) was determined to be approximately 1.439 $\Omega \cdot cm^2$. This parameter directly influenced the power delivery capability of the supercapacitor. The fitted polarization resistance (Rp), CPEdl, and CPE exponent (n) values were calculated as 1.372×10^6 $\Omega \cdot cm^2$, 34.13×10^{-6} $\Omega^{-1} \cdot s \cdot cm^{-2}$, and 0.918, respectively. The CPE exponent value close to unity indicated nearly capacitive behavior, although slight deviations confirmed surface heterogeneity. Correspondingly, the EIS analysis demonstrated that Fe incorporation reduced interfacial resistance and improved charge transfer properties. Therefore, the impedance results further supported the enhanced electrochemical performance observed in CV and GCD measurements..

Conclusion

In this study, CuO nanostructured thin films, both pure and Fe-doped, were successfully synthesized on ITO substrates through the ultrasonic spray pyrolysis technique. The prepared films were systematically evaluated in terms of their structural, morphological, optical, and electrochemical properties. The formation of the monoclinic CuO phase was confirmed by XRD analysis. With increasing Fe concentration, noticeable changes in diffraction peak intensity and crystallite size were observed. In addition, secondary phase reflections related to Fe oxide were detected at higher doping levels. The calculated structural parameters indicated a reduction in crystallite size along with an increase in dislocation density and microstrain, demonstrating that Fe incorporation introduced lattice distortion. The SEM observations revealed that the undoped CuO films exhibited polyhedron-like grains with mixed orientations. After Fe doping, grain growth became more pronounced and surface morphology was modified. The elemental mapping and EDX analyses verified the uniform distribution of Fe within the

CuO matrix, confirming successful incorporation of the dopant. The photoluminescence measurements demonstrated characteristic emission bands corresponding to near-band-edge and defect-related transitions. A reduction in PL intensity was observed after Fe incorporation, indicating modifications in defect concentration and recombination dynamics. UV–Vis analysis showed that optical absorbance increased with Fe doping, while the band gap slightly shifted toward higher energy values. Electrochemical measurements revealed that Fe doping significantly improved charge storage behavior. The Fe-doped CuO electrode exhibited higher specific capacitance values compared to the undoped sample, particularly at lower scan rates and current densities. GCD and EIS analyses further confirmed improved charge transfer characteristics and reduced interfacial resistance in the doped system. Fe incorporation effectively enhanced the electrochemical performance and modified the electronic as well as structural properties of the CuO thin films, as demonstrated by the overall results. Therefore, as promising candidates for supercapacitor applications were considered the Fe-doped CuO nanostructured thin films synthesized via the USP technique.

References

[1] G.G. Welegergs, Z.M. Mehabaw, H.G. Gebretinsae, M.G. Tsegay, L. Kotsedi, Z. Khumalo, N. Matinisie, Z.T. Aytuna, S. Mathur, Z.Y. Nuru, S. Dube, M. Maaza, "Electrodeposition of nanostructured copper oxide (CuO) coatings as spectrally solar selective absorber: Structural, optical and electrical properties", Infrared Physics and Technology 133 (2023) 104820.

[2] V. Arjun, K.P. Muthukumaran, K. Ramachandran, A. Nithya, S. Karuppuchamy, "Fabrication of efficient and stable planar perovskite solar cell using copper oxide as hole transport material", Journal of Alloys and Compounds 923 (2022) 166285.

[3] R. Saad, K. Abdelkarem, A.M. Ahmed, M. Zayed, Z.M. Faidey, M. Shaban, M.T. Tammam, H. Hamdy, "Enhanced CO_2 gas sensing at room temperature using Ag-plated Na-doped CuO thin films synthesized by successive ionic layer adsorption and reaction technique" Surfaces and Interfaces 44 (2024) 103789.

[4] S.B. Wang, C.H. Hsiao, S.J. Chang, K.T. Lam, K.H. Wen, S.J. Young, S.C. Hung, B.R. Huang, "CuO nanowire-based humidity sensor", IEEE Sensors Journal 12 (2012) 1884–1888.

[5] H.U. Habermeier, "Science and technology of cuprate-based high temperature superconductor thin films, heterostructures and superlattices—the first 30 years" Low Temperature Physics 42 (2016) 840–862.

[6] D.P. Dubal, G.S. Gund, C.D. Lokhande, R. Holze, “CuO cauliflowers for supercapacitor application: Novel potentiodynamic deposition” Materials Research Bulletin 48 (2013) 923–928.

[7] Kasapoğlu, Ahmet Emre, Saman Habashyani, Ali Baltakesmez, Demet İskenderoğlu, and Emre Gür. "The effect of the change in the amount of Sb doping in ZnO nanorods for hydrogen gas sensors." International Journal of Hydrogen Energy 46, no. 41 (2021): 21715-21725.

[8] Turgut, G., S. Aydogan, Mehmet Yilmaz, A. Özmen, and H. Kacus. "An investigation of spray deposited CdO films and CdO/p-Si heterojunction at different substrate temperatures." JOM 73, no. 2 (2021): 566-573.

[9] Tursucu, A., S. Aydogan, A. Kocyigit, A. Ozmen, and M. Yilmaz. "Investigation the Performance of Cr-Doped ZnO Nanocrystalline Thin Film in Photodiode Applications." Jom 74, no. 3 (2022): 777-786.

[10] LI, Youxia, et al. Structural and room-temperature ferromagnetic properties of Fe-doped CuO nanocrystals. Journal of Applied Physics, 2010, 107.11.

[11] CHAFI, Fatima Zahra, et al. Fe-doped CuO deposited by spray pyrolysis technique. In: 2015 3rd International Renewable and Sustainable Energy Conference (IRSEC). IEEE, 2015. p. 1-5.

[12] YILDIZ, Tülay; KATI, Nida; GÜL, Büşra. Examination of Structural and Electrical Properties of CuO-Doped CdO Nanocomposites Produced by the Hydrothermal Method. Crystal Research and Technology, 2022, 57.10: 2200093.

[13] Iqbal Singha, R.K. Bedi, Studies and correlation among the structural, electrical and gas response properties of aerosol spray deposited self assembled nanocrystalline CuO, Applied Surface Science 257 (2011) 7592–7599.

[14] T.V. Thi, A.K. Rai, J. Gim, J. Kim, Potassium-doped copper oxide nanoparticles synthesized by a solvothermal method as an anode material for high-performance lithium ion secondary battery, Appl. Surf. Sci., 305 (2014), pp. 617-625.

[15] S.K. Shinde, D.P. Dubal, G.S. Ghodake, P. Gomez-Romero, S. Kim, V.J. Fulari, Influence of Mn incorporation on the supercapacitive properties of hybrid CuO/Cu (OH) 2 electrodes, RSC Adv., 5 (2015), pp. 30478-30484.

[16] CHAUDHARY, Manika, et al. Experimental investigation of Co and Fe-Doped CuO nanostructured electrode material for remarkable electrochemical performance. Ceramics International, 2021, 47.2: 2094-2106.

[17] Buppachat Toboonsung, Pisith Singjai, Formation of CuO nanorods and their bundles by an electrochemical dissolution and deposition process, Journal of Alloys and Compounds 509 (2011) 4132–4137

[18] ERDOĞAN, İbrahim Y.; GÜLLÜ, Ömer. Optical and structural properties of CuO nanofilm: its diode application. Journal of Alloys and Compounds, 2010, 492.1-2: 378-383.

[19] CHANG, Sung-Sik; LEE, Hyung-Jik; PARK, Hye Jeong. Photoluminescence properties of spark-processed CuO. Ceramics international, 2005, 31.3: 411-415.

[20] LIN, Hung-Hsiao, et al. Characterizing well-ordered CuO nanofibrils synthesized through gas-solid reactions. Journal of applied physics, 2004, 95.10: 5889-5895.

[21] SON, Dong Ick; YOU, Chan Ho; KIM, Tae Whan. Structural, optical, and electronic properties of colloidal CuO nanoparticles formed by using a colloid-thermal synthesis process. Applied surface science, 2009, 255.21: 8794-8797.

[22] HUANG, C.-Y., et al. Photoluminescence properties of a single tapered CuO nanowire. Applied surface science, 2010, 256.11: 3688-3692.

[23] JIN, Changhyun, et al. Influence of SnO2 coating and thermal annealing on the structure and luminescence properties of CuO nanorods. Solid State Communications, 2010, 150.37-38: 1812-1817.

[24] ASLANI, Alireza; OROOJPOUR, Vahid. CO gas sensing of CuO nanostructures, synthesized by an assisted solvothermal wet chemical route. Physica B: Condensed Matter, 2011, 406.2: 144-149.

[25] ASLANI, Alireza. Controlling the morphology and size of CuO nanostructures with synthesis by solvo/hydrothermal method without any additives. Physica B: Condensed Matter, 2011, 406.2: 150-154.

[26] CHANG, Sung-Sik; LEE, Hyung-Jik; PARK, Hye Jeong. Photoluminescence properties of spark-processed CuO. Ceramics international, 2005, 31.3: 411-415.

[27] SOLACHE-CARRANCO, H., et al. Photoluminescence and X-ray diffraction studies on Cu2O. Journal of Luminescence, 2009, 129.12: 1483-1487.

[28] GAO, Pan, et al. X-ray excited luminescence of cuprous iodide single crystals: On the nature of red luminescence. Applied Physics Letters, 2009, 95.22.

[29] W. Lu, L.T. Qu, K. Henry, L.M. Dai, High performance electrochemical capacitors from aligned carbon nanotube electrodes and ionic liquid electrolytes, J Power Sources, 189 (2009) 1270-1277.

[30] VANNATHAN, Anjana Anandan, et al. Polyoxovanadate-Activated Carbon-Based Hybrid Materials for High-Performance Electrochemical Capacitors. Journal of The Electrochemical Society, 2022, 169.5: 050538.

[31] V.V. Chernyavina, A.G. Berezhnaya, A.V. Panchenko, Nanoparticles of Nickel Hexacyanoferrate Derivatives as the Components of Electrode Materials for Electrochemical Capacitors, Russ J Electrochem+, 58 (2022) 74-82.

[32] XU, Shichen; WU, Mingmao; ZHANG, Jin. Ultrafast Electrochemical Capacitors with Carbon Related Materials as Electrodes for AC Line Filtering. Chemistry–A European Journal, 2022, 28.31: e202200237.

[33] W.B. Lv, L. Li, Q.H. Meng, X.T. Zhang, Molybdenum-doped CuO nanosheets on Ni foams with extraordinary specific capacitance for advanced hybrid supercapacitors, J Mater Sci, 55 (2020) 2492-2502.

[34] J.S. Shaikh, R.C. Pawar, R.S. Devan, Y.R. Ma, P.P. Salvi, S.S. Kolekar, P.S. Patil, Synthesis and characterization of Ru doped CuO thin films for supercapacitor based on Bronsted acidic ionic liquid, Electrochim Acta, 56 (2011) 2127-2134.

[35] J.C. Huang, H.B. Wu, D.X. Cao, G.L. Wang, Influence of Ag doped CuO nanosheet arrays on electrochemical behaviors for supercapacitors, Electrochim Acta, 75 (2012) 208-212.

[36] L. Arun, C. Karthikeyan, D. Philip, M. Sasikumar, E. Elanthamilan, J.P. Merlin, C. Unni, Effect of Ni2+ doping on chemocatalytic and supercapacitor performance of biosynthesized nanostructured CuO, J Mater Sci-Mater El, 29 (2018) 21180-21193.

[37] M. Chaudhary, M. Singh, A. Kumar, Prachi, Y.K. Gautam, A.K. Malik, Y. Kumar, B.P. Singh, Experimental investigation of Co and Fe-Doped CuO nanostructured electrode material for remarkable electrochemical performance, Ceram Int, 47 (2021) 2094-2106.

Figure 1. XRD results of undoped and Fe doped CuO thin films

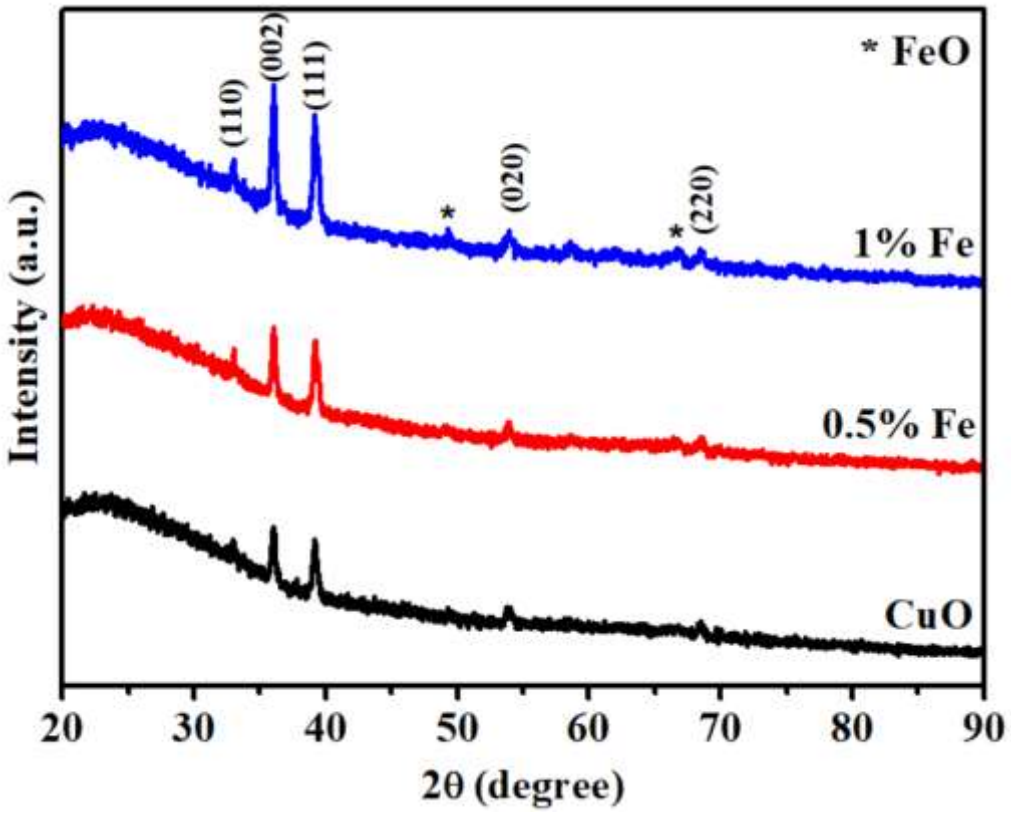


Figure 2. SEM images and EDAX results of undoped and Fe doped CuO thin films.

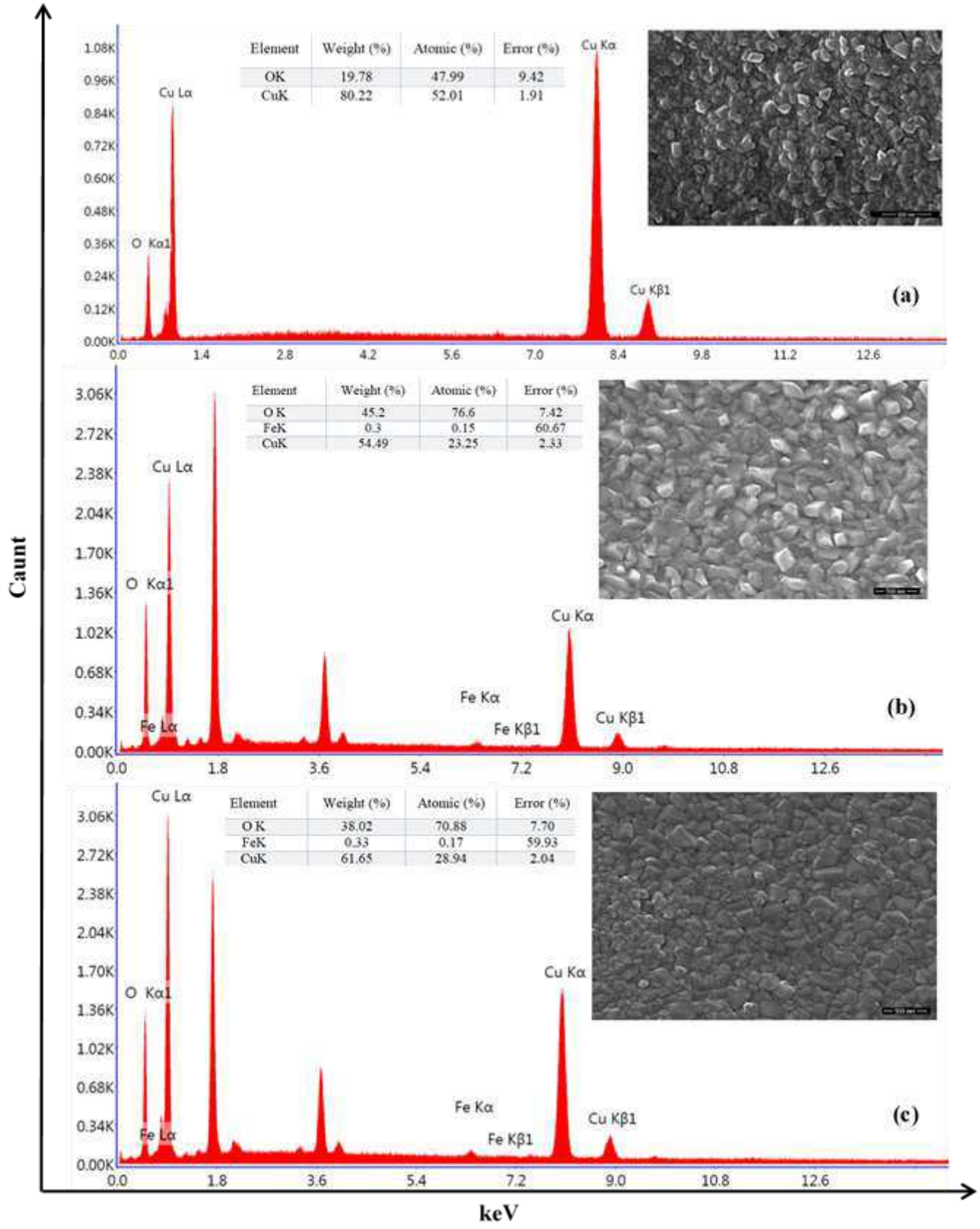


Figure 3. The photoluminescence spectra of undoped and Fe doped CuO thin films.

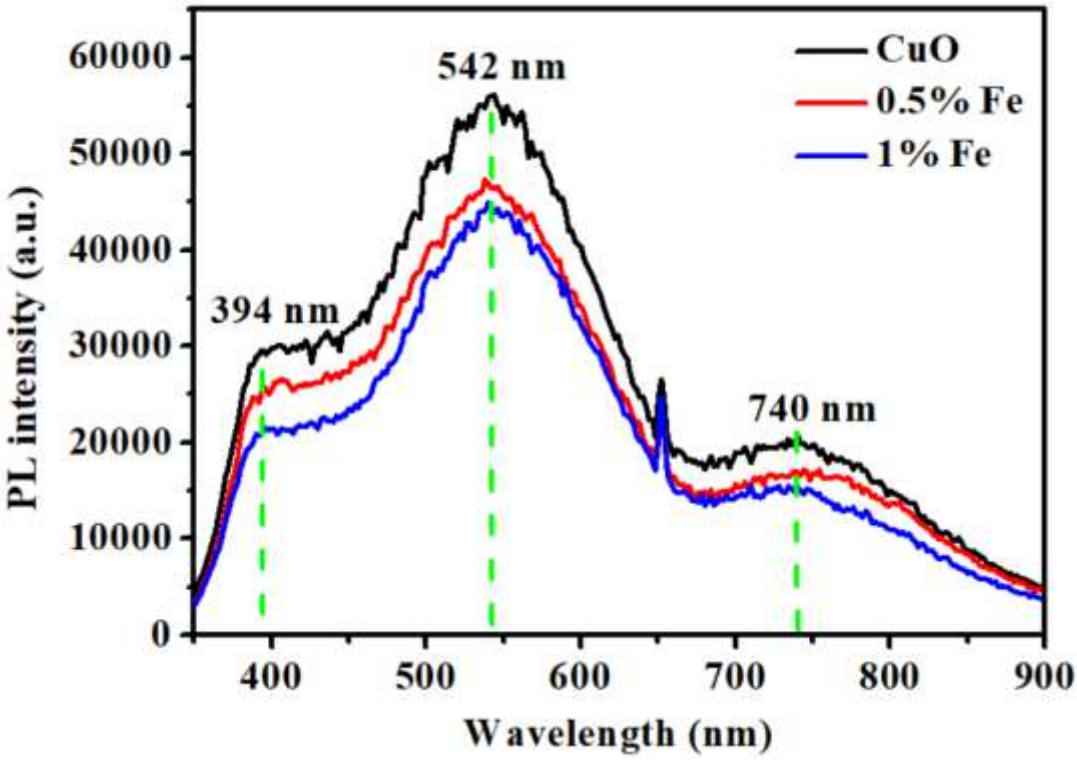
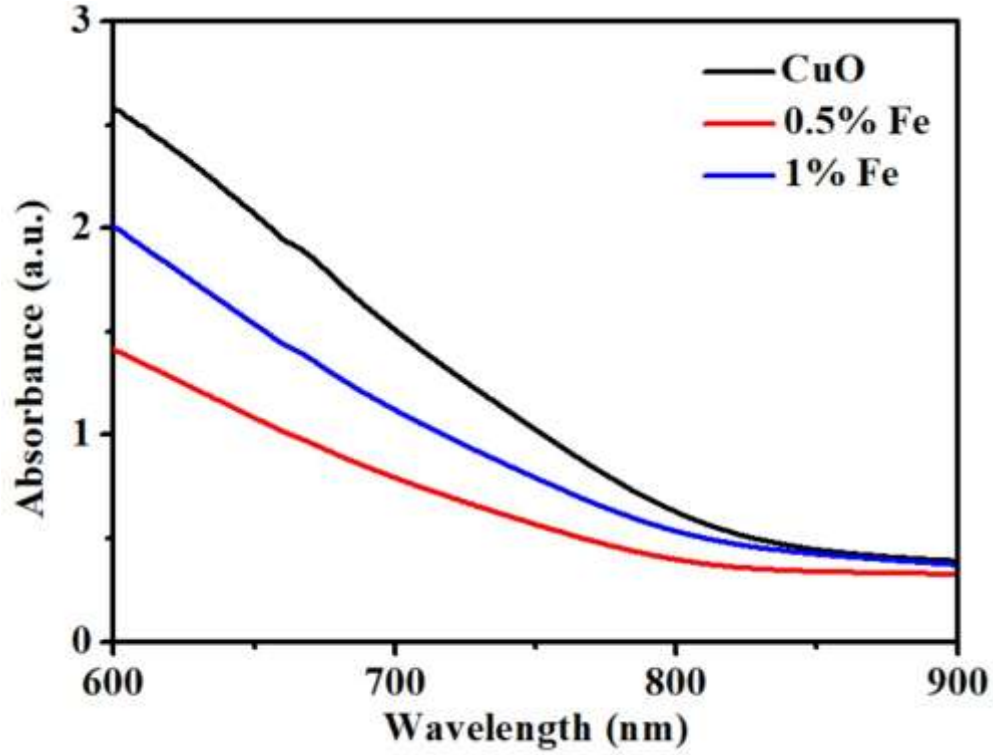


Figure 4. The absorbance spectra of undoped and Fe-doped CuO nanostructured thin films.



\

Figure 5. The optical band gap energies of undoped and Fe-doped CuO nanostructured thin films.

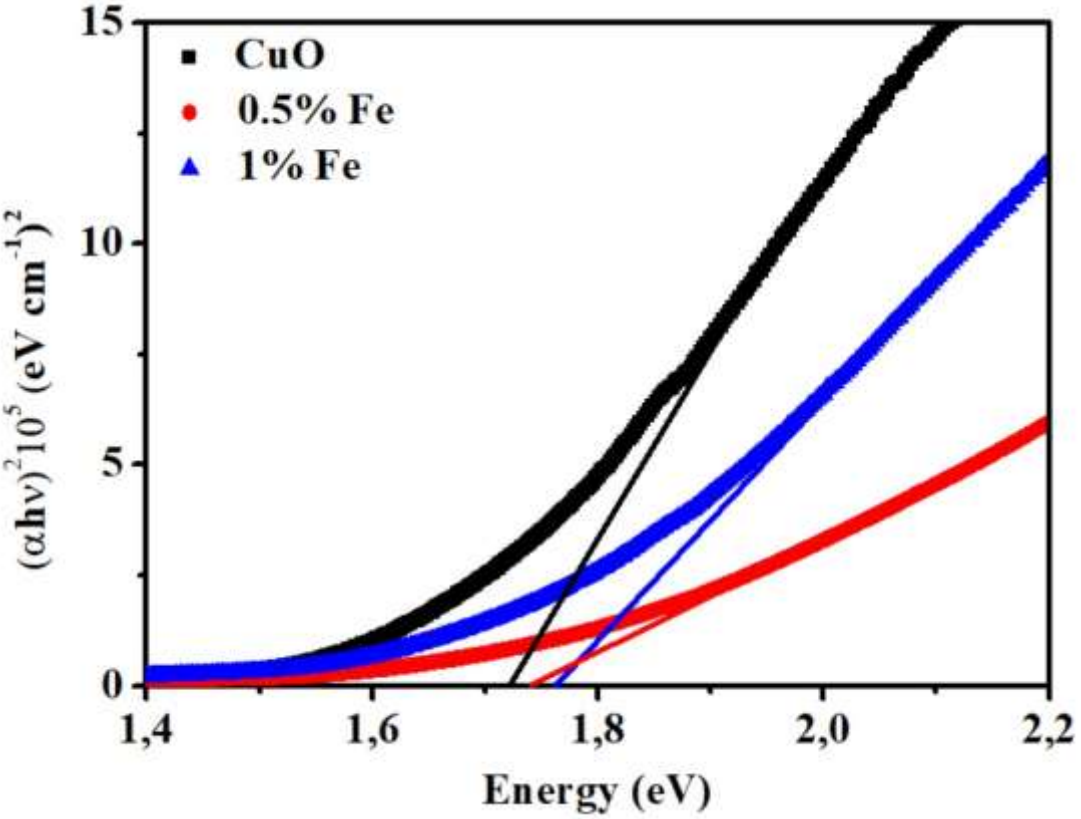


Figure 6: CV plot of (a) undoped (b) and 1% Fe doped CuO (c) spesific capacitance of undoped and 1% Fe doped thin films electrode deposited on ITO substrate

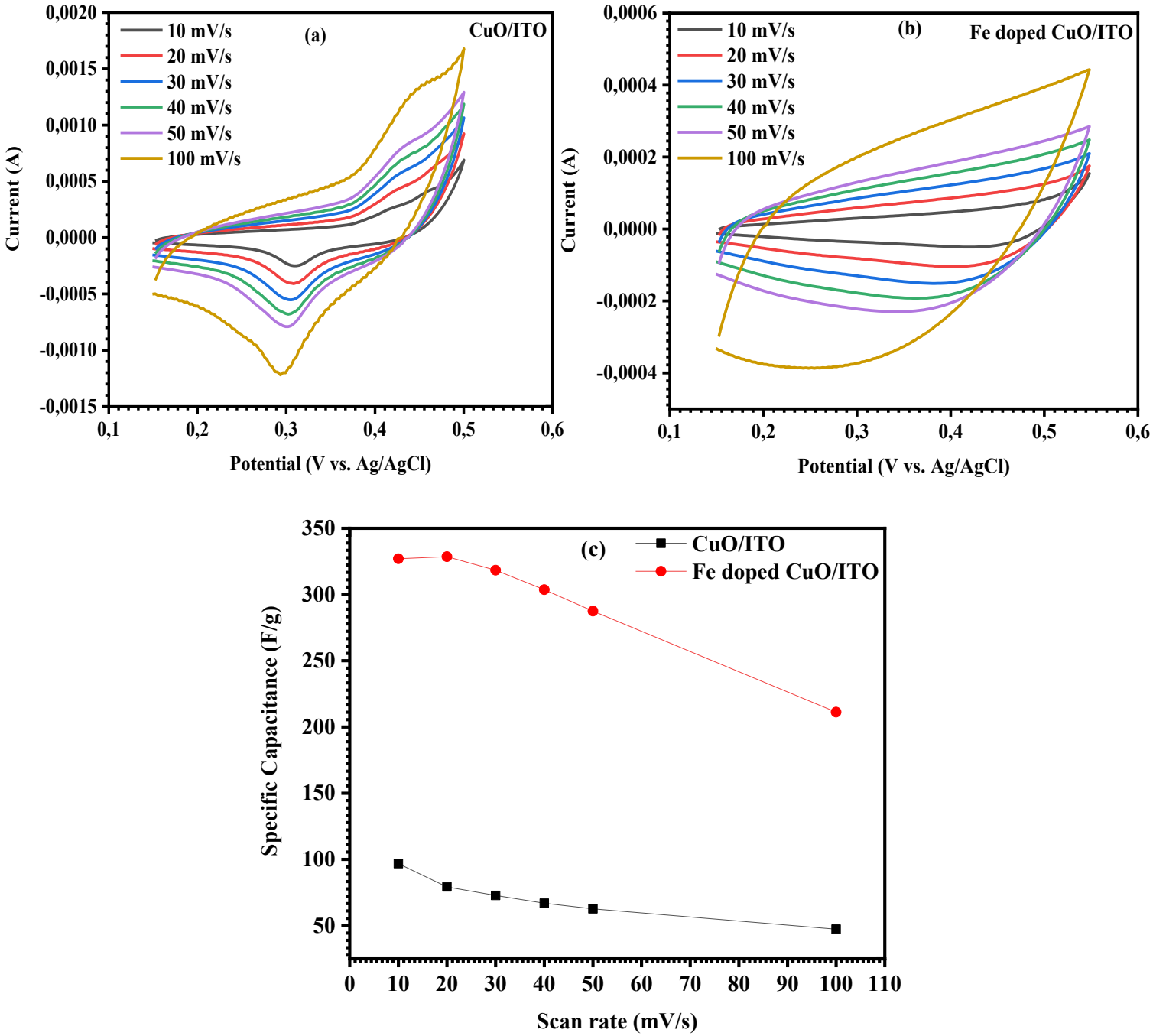


Figure 7: Charge-discharge curve of (a) undoped (b) 1% Fe doped CuO nanostructure electrode at 1A/g current density (electrolyte: 1M KOH, reference electrode: Ag/AgCl, saturated KCl) **(c)** Electrochemical impedance spectrum of the Fe doped CuO electrode

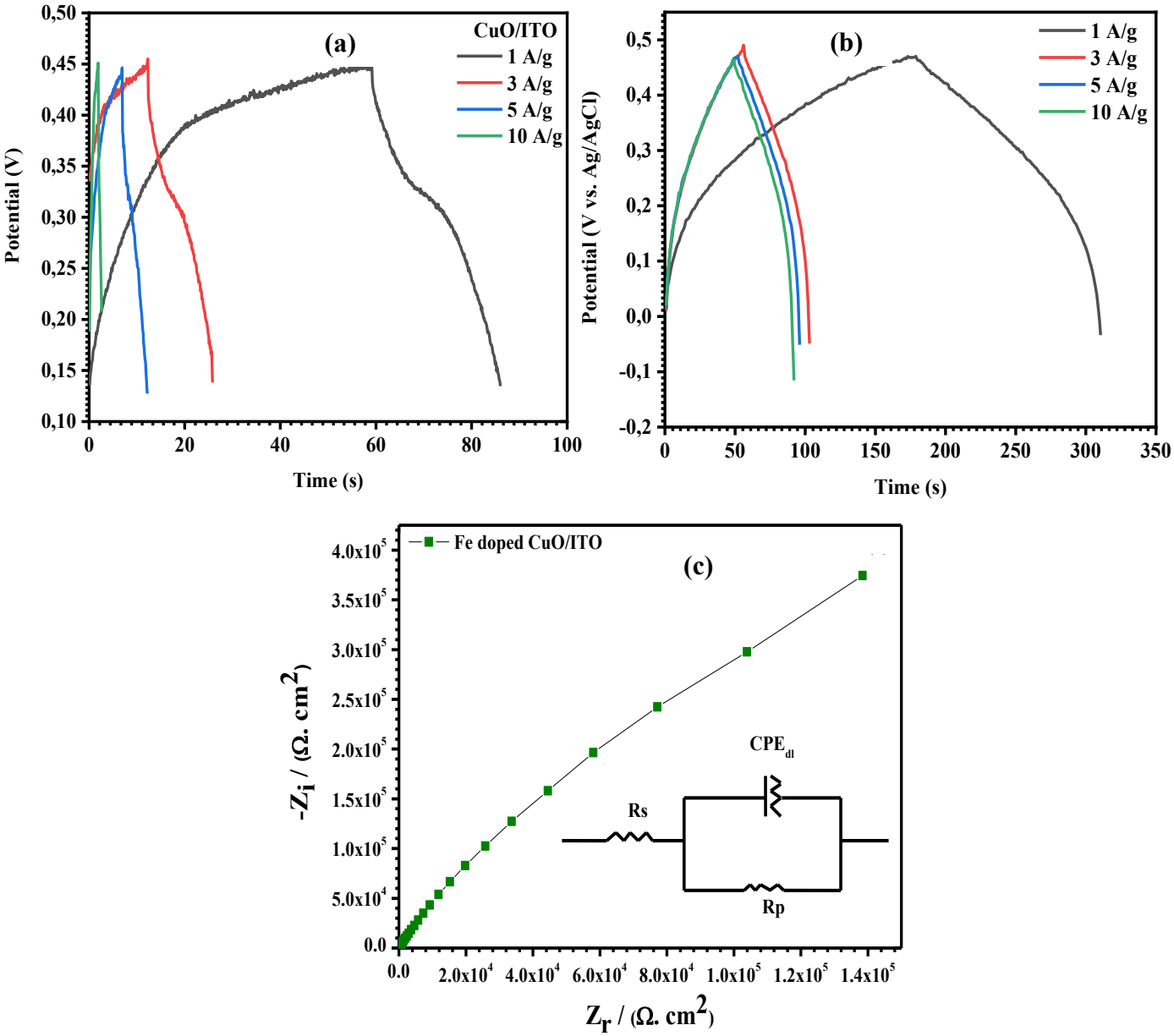


Table 1. E_g and XRD parameters (β, d-spacing, D, δ, ε) of undoped and Fe doped CuO thin films

Sample name	Eg (eV)	Pos. (°2θ)	*β* (°2θ)	*d*-spacing (Å)	*D* (nm)	δ (10^4 nm^{-2})	ε (10^{-3} %)
CuO	1.72	36.05	0.28	2.489	54.98	3.31	66
0.5% Fe	1.74	35.06	0.29	2.557	53.10	3.55	68
1% Fe	1.76	36.06	0.35	2.489	43.02	5.40	84

Table 2. Specific Capacitance values from CV and GCD versus scan rate and current density of undoped and 1% Fe doped CuO thin films

	Specific Capacitance values from CV		Specific Capacitance values from GCD		
Scan rate (mV/s)	CuO (F/g)	Fe doped CuO (F/g)	CuO (F/g)	Fe doped CuO (F/g)	Current Density (A/g)
10	96	327	77	330	1
20	79	328	37	120	3
30	72	318	15	112	5
40	66	303	2	107	10
50	62	287			
100	47	211			